Geochimica et Cosmochimica Acta 365 (2024) 202–214

Contents lists available at ScienceDirect

Geochimica et Cosmochimica Acta

journal homepage: www.elsevier.com/locate/gca

High-precision zirconium isotope analysis of Pacific seawater reveals large mass-dependent fractionations in the ocean

Linqing Huang [a,*], François L.H. Tissot [b], Mauricio Ibañez-Mejia [c], Kiefer O. Forsch [a], Carli Arendt [d], C. Anela Choy [a], Sarah M. Aarons [a]

[a] Scripps Institution of Oceanography, University of California San Diego, La Jolla, CA 92093, USA
[b] The Isotoparium, Division of Geological and Planetary Sciences, California Institute of Technology, Pasadena, CA 91125, USA
[c] Department Geosciences, University of Arizona, Tucson, AZ 85721, USA
[d] Department of Marine, Earth, & Atmospheric Sciences, North Carolina State University, Raleigh, NC 27695, USA

ARTICLE INFO

Associate editor: Yoshiki Sohrin

Keywords:
Zr isotopes
Pacific Ocean
Water mass tracer
Particle scavenging

ABSTRACT

Zirconium (Zr) stable isotopes recently emerged as potential tracers of magmatic processes and, as a result, their behavior in high-temperature environments have been the focus of extensive characterization. In contrast, few studies have focused on Zr behavior and isotopic fractionation in low temperature or aqueous environments. Here, we describe a new analytical routine for highly precise and accurate analysis of Zr isotopes of water samples, using a combination of double-spike and iron co-precipitation methods. To assess the impact of potential systematic biases a series of experiments were conducted on natural and synthetic water samples. Our results show that the spike-to-sample ratio, matrix composition, and high field-strength element (HFSE) concentration have negligible effects on measured seawater Zr isotopic compositions, and that the Fe co-precipitation method used yields accurate and precise Zr isotope data. We thus apply this method to natural seawater samples collected from a water column profile in the Pacific Ocean off the coast of California, with depths ranging from 5 to 711 m. We find that the natural seawater samples are highly fractionated relative to solid-Earth values and display marked variability in $\delta^{94/90}$Zr as a function of depth, ranging from ~ +0.650 ‰ near the surface, to + 1.530 ‰ near the profile bottom, with an analytical uncertainty of ± ~0.045 ‰ (2 SE, external reproducibility). The $\delta^{94/90}$Zr value of seawater is much higher than that of Earth's mantle and continental crust, which has a $\delta^{94/90}$Zr value near zero, indicating the presence of processes in the hydrosphere capable of inducing large mass-dependent fractionation. Furthermore, the seawater $\delta^{94/90}$Zr value exhibits systematic variations with respect to water depth and salinity, suggesting that Zr isotopic compositions may be sensitive to seawater chemical properties and source highlighting its potential utility as a tracer of biogeochemical processes within the ocean.

1. Introduction

Zirconium (Zr) is an incompatible high field-strength element (HFSE) whose concentration in igneous rocks has long been used to study the differentiation of silicate magmatic systems (Kelemen et al. 1990; Xie et al. 1993; David et al. 2000; Weyer et al. 2003; Münker et al. 2004; Claiborne et al. 2006; Pfänder et al. 2007). Recently, the discovery of isotopic variations in accessory phases (Ibanez-Mejia & Tissot 2019) and bulk rocks (Inglis et al., 2019) has raised the possibility that Zr stable isotopes could also be used as tracers of magmatic processes. As a result, numerous studies have investigated the Zr isotope systematics in high-temperature terrestrial environments (Ibañez-Mejia & Tissot 2019; Inglis et al. 2019; Chen et al. 2020; Guo et al. 2020; Tian et al. 2020; Wu et al. 2020; Aarons et al. 2021; Méheut et al. 2021; Bindeman & Melnik 2022; Guo et al. 2022; Jiao et al. 2022; Zhu et al. 2023; Tompkins et al. 2023), and, to a much lesser extent, low temperature environments (Tian et al. 2021; Klaver et al. 2021). In sharp contrast, no constraints yet exist on the composition and distribution (*i.e.*, homogeneity/heterogeneity) of Zr stable isotopes in the hydrosphere.

Like all HFSEs, Zr has extremely low solubility in aqueous fluids and has a short residence time in the ocean (~3700 yr) (Firdaus et al. 2011), despite its high abundance in Earth's continental crust (Orians & Merrin

* Corresponding author.
E-mail address: lih007@ucsd.edu (L. Huang).

https://doi.org/10.1016/j.gca.2023.11.018
Received 9 May 2023; Accepted 22 November 2023
Available online 25 November 2023

2001). Unlike in high-T environments however, where HFSEs have nearly identical geochemical behaviors, elemental fractionation of HFSE is well documented in the modern ocean (Firdaus et al. 2008; Firdaus et al. 2011). In particular, Zr and its "geochemical twin" hafnium (Hf) (Frank, 2011), which has the same valence (+4) and similar ionic radii (0.83 and 0.84 Å respectively (Shannon, 1976)), have been shown to be strongly fractionated in seawater, where the Hf/Zr ratio varies between 45 and 350 (in contrast to the near chondritic value of ~ 35–40 observed in most crustal and mantle materials (Goldschmidt, 1937; Hoskin & Schaltegger 2003)). These extreme Zr/Hf variations are thought to be driven by rapid removal of Zr from seawater through adsorption onto sinking particles (Firdaus et al. 2011; Schmidt et al. 2014). Any isotopic fractionation accompanying such elemental fractionation could (i) result in significant Zr isotope variations, and (ii) be leveraged to understand the mechanism driving the decoupling of Zr and Hf in Earth's Ocean. The potential therefore exists for Zr isotopes to be a useful oceanographic tracer.

While a multitude of methods now exist for the determination of Zr stable isotope compositions in solid geological materials (Inglis et al. 2018; Zhang et al. 2019; Tompkins et al. 2020; He et al. 2021; Zhang et al. 2022; Xie et al. 2023), measuring the isotopic composition of dissolved Zr in the ocean presents a major analytical challenge. Indeed, Zr concentrations in seawater vary between ~ 50–250 pmol kg^{-1} (4.6–23 ng/L) (McKelvey & Orians 1993; Firdaus et al. 2008), thus requiring the processing of ~ 10–20 L of seawater per sample to obtain sufficient Zr for high-precision isotope analysis. Here, we introduce a new analytical technique for analysis of mass-dependent Zr isotopic compositions in seawater using a combination of iron (Fe) co-precipitation and double-spike MC-ICP-MS methods. One of the key benefits of using this technique is that it enables the recovery of over 90 % of HFSE from the solution through adsorption into Fe precipitates. As a result, HFSEs become highly enriched in the Fe-hydroxide precipitates compared to seawater and can be more easily purified to obtain enough Zr for isotopic measurements. Below, we present the details of this new method, including a series of experiments performed using synthetic seawater doped with varying amounts of Zr of known isotopic composition designed to determine the effects of Fe co-precipitation on the measured Zr isotopic composition. We then apply this new approach to seawater samples from the Pacific Ocean. We find that, (i) our method produces accurate and precise Zr isotope data for seawater of varying concentrations and over a range of double spike proportions, (ii) the Fe co-precipitation preconcentration technique does not impart measurable Zr isotopic fractionation to natural water samples, and (iii) Zr is markedly fractionated in the ocean and exhibits systematic correlations with depth transect and with respect to salinity. As such, this study highlights the potential utility of Zr stable isotopes as a tracer of water masses and biogeochemical processes in the ocean.

2. Materials and methods

2.1. Reagents, labware cleaning & blanks

All laboratory work was carried out within class 100 laminar flow workstations in clean labs at Scripps Institution of Oceanography (SIO), the Arizona Heavy Isotopes Laboratory (AHIL) at University of Arizona, and the Isotoparium at the California Institute of Technology. Chemical reagents to process the samples included MilliQ water, HCl, HNO_3, HF, and H_2O_2. All acids used were prepared by double sub-boiling distillation of analytical grade acids using Savillex® DST-1000 systems. Because of the low levels of Zr in seawater, blanks were closely monitored. Blank values for the undiluted stock acids are reported in Table 1 and are all below 0.1 pg Zr per mL of acid.

Polyethylene carboy containers for water collection were precleaned in a clean laboratory at SIO prior to sample collection to minimize the need for blanks. The 10 and 20 L collapsible polyethylene carboys (Fisher Scientific, Wayne, MI, USA) were triple rinsed with MilliQ water, leached for 48 hrs with 2 L of 10 % trace grade HNO_3, triple rinsed with MilliQ water, leached for 48 hrs with 2 L of 10 % double distilled HCl and triple rinsed with MilliQ water. Polypropylene centrifuge tubes and bottles (15 mL and 1 L) used in the pre-concentration step were cleaned with analytical grade 10 % HNO_3, HCl, and double distilled 10 % HNO_3 at 60° C.

Table 1
Reagents used for the chemical processing of samples and corresponding Zr blanks.

	Product	Purification method	Zr blank (pg mL^{-1})
MQ water	Millipore, 18.2 MΩ		< 0.1
HCl	ACS grade, 37 %	Double infrared distillation	< 0.1
HNO_3	ACS grade, 65 %	Double infrared distillation	< 0.1
HF	Optima grade, 48 %		<0.05
H_2O_2	Optima grade, 30 %		<0.05
$FeCl_3{\cdot}6H_2O$	Solid	Back extraction	< 1.0
$NH_4{\bullet}OH$	Optima grade, 25 %		<0.05

The sample vials used for chemical digestion and dissolution (PFA vials from Savillex) were pre-cleaned in a four-step procedure. First, they were cleaned thoroughly with analytical grade ethanol and subsequently rinsed several times with distilled water. The second and third steps involved boiling in analytical grade 4 M HNO_3 and 3 M HCl. As a final step, the vials were filled halfway with a mixture of double-distilled concentrated HNO_3 and HF and capped for 3 days on a hot plate at 110° C. The vials were thoroughly rinsed with MilliQ water between each acid cleaning step and at the end of the entire procedure.

To determine the level of laboratory contamination introduced by our Fe co-precipitation and chemical purification methods two blanks were produced: a total procedural blank (TPB) and an "NaCl" blank. The TPB blank consisted of 20 L of MilliQ water with Zr double-spike added to determine the blank arising from both the Fe co-precipitation and subsequent chemical processing, and the NaCl blank consisted in 40 L of MilliQ water with 3.5 % ultrapure NaCl to determine the blank contributed from NaCl used in synthetic seawater. Both blank loads underwent the complete chemical processing procedure, their Zr isotopic compositions were measured alongside other samples, and the mass of the Zr blank was calculated using isotope dilution.

2.2. Artificial seawater preparation

Multiple artificial seawater samples were prepared to assess the recovery yields of our sample processing protocols, as well as the accuracy and precision of the seawater Zr isotope data. Nine artificial water samples were prepared using ultrapure deionized water (MilliQ, 18.2 MΩ) and 3.5 % ultrapure sodium chloride, in pre-cleaned carboys to mimic those collected in open ocean natural environments (see Table 2 for details). In addition, a "freshwater" sample of 20 L of MilliQ water was also prepared to compare the matrix effect on Fe co-precipitation. The prepared water samples were then acidified with double-distilled HCl to a pH between 2 and 3 to prevent adsorption of elements onto the walls of the containers, which would decrease the recovery yield. Aliquots of NIST RM8299 Zr isotope reference material were then added to the artificial water samples (Tissot et al. 2023). Each sample was then shaken vigorously and left to sit for at least 24 h so that it would reach homogenous Zr concentrations throughout the water.

2.3. Natural seawater sampling

Natural seawater samples were collected on the R/V *Robert Gordon Sproul* from the Pacific Ocean off the coast of California in February

Table 2
Description of natural and artificial seawater samples.

Sample name	Spike before coprecipitation?	Volume (L)	Description
Sproul-5 m-B	Yes	20	Seawater collected at 5 m water depth
Sproul-5 m-A	No	20	Seawater collected at 5 m water depth
Sproul-20 m-B	Yes	20	Seawater collected at 20 m water depth
Sproul-20 m-A	No	20	Seawater collected at 20 m water depth
Sproul-50 m-A	No	20	Seawater collected at 50 m water depth
Sproul-300 m-B	Yes	10	Seawater collected at 300 m water depth
Sproul-300 m-A	No	10	Seawater collected at 300 m water depth
Sproul-711 m-B	Yes	10	Seawater collected at 711 m water depth
Sproul-711 m-A	No	10	Seawater collected at 711 m water depth
Seawater 1-B	Yes	10	Synthetic seawater + Zr (100 pmol kg^{-1})
Seawater 2-A	No	10	Synthetic seawater + Zr (100 pmol kg^{-1})
Surface water	Yes	20	Synthetic seawater + Zr (25 pmol kg^{-1})
Bottom water	Yes	10	Synthetic seawater + Zr (250 pmol kg^{-1})
Seawater V1	Yes	6	Synthetic seawater + Zr (100 pmol kg^{-1})
Seawater V2	Yes	10	Synthetic seawater + Zr (100 pmol kg^{-1})
Seawater V3	Yes	14	Synthetic seawater + Zr (100 pmol kg^{-1})
Pier seawater-B	Yes	40	Coastal water collected at 5 m water depth.
Pier seawater-A	No	40	Coastal water collected at 5 m depth.
Freshwater	Yes	20	MQ H_2O + Zr (100 pmol kg^{-1}),
TPB	Yes	40	MQ H_2O, no Zr, blank sample
NaCl blank	Yes	40	Synthetic seawater, no Zr, NaCl blank

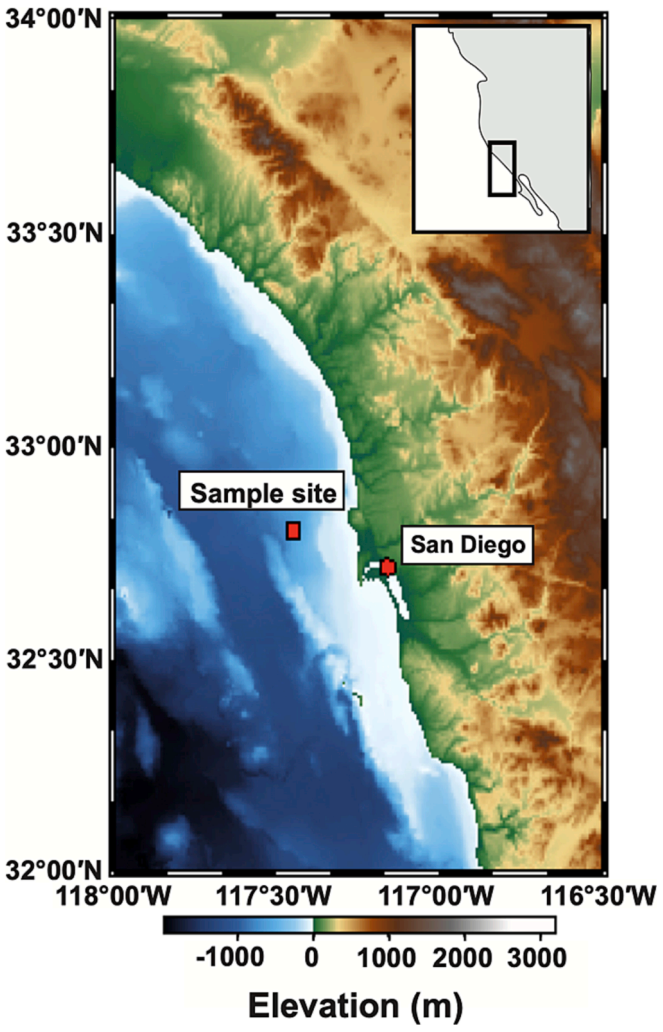

Fig. 1. Map indicating the sampling location in the Pacific Ocean, off the coast of S. California. Regional location shown in the inset map depicting the western United States.

2022 (32° 47.858′N, 117° 28.283′ W, Fig. 1). Hydrographic data were collected with a SeaBird Electronics profiling conductivity, temperature, depth (CTD) sensor package. Depth discrete seawater samples were collected using Niskin bottle-type rosette sampler, equipped with 12-L Niskin bottles. Upon completion of the CTD cast, seawater samples were immediately drained into acid precleaned carboys. Seawater was sampled at depths of ~ 5 m (40 L), 20 m (40 L), 50 m (20 L), 300 m (20 L) and 711 m (20 L). Within 24 h, 20 to 40 L of seawater were filtered through 0.2 μm Acropak-200 capsule filters pressurized by filtered air at SIO and stored in acid pre-cleaned 20 L polypropylene carboys. Immediately following filtration, natural seawater samples were acidified to a pH of 2–3 until the Fe co-precipitation step.

2.4. Iron co-precipitation & sample digestion

To gauge the potential effects of Fe co-precipitation and metal concentration techniques on the measured Zr isotopic fractionation in both natural and artificial seawater samples, a series of experiments were performed (Table 2). For both natural and artificial waters, the workflow for sampling, chemical processing, digestion, and column chemistry are described in Fig. 2. These protocols are adapted from previously established methods of concentrating and isolating trace amounts of metals in large volumes of seawater such as Hf and neodymium (Nd) through the removal of Fe precipitate from the sample (Rickli et al. 2009; Arendt et al. 2015). For the Fe precipitate, Fisher brand I88–500 GSA/VA ferric chloride hexahydrate ($FeCl_3{\cdot}6H_2O$) was precleaned using a back extraction method involving diethyl-ether, double distilled 6 M HCl, and MilliQ water described in Arendt et al. (2015). The purified $FeCl_3$ was dissolved in 3 M HCl at an Fe concentration of 0.2 g mL^{-1} of solution. An aliquot of the resulting solution, sized to achieve a final concentration of 6 mg Fe kg^{-1} water in the sample, was added to the acidified water samples. Samples were then shaken vigorously and left to sit for 24 h to allow for chemical equilibrium. Once the added Fe was stable and homogenous in solution, ammonium hydroxide ($[NH^{4+}][OH^{-}]$) solution was added to the sample to raise the pH to approximately 8–9. Upon raising the solution pH, Fe hydroxide precipitation was induced and allowed to proceed over the course of 2 days. After settling of the precipitate (typically ~ 72 hr), the supernatant was decanted, and the recovered Fe precipitates along with co-precipitated metals were separated from the residual water by centrifugation. To eliminate excess salts in the seawater samples prior to digestion, Fe precipitates (0.5 to 4 g) were rinsed five times with MilliQ water (20 to 40 mL) that had been buffered with ammonium hydroxide to a pH of 9. Samples were then transferred to 20 mL Teflon beakers and evaporated to dryness on a hot plate at 130 °C. Finally, samples were treated with aqua regia, tightly capped and heated to 130 °C to eliminate organic matter. Once almost dried down, the samples were treated with 1 mL of

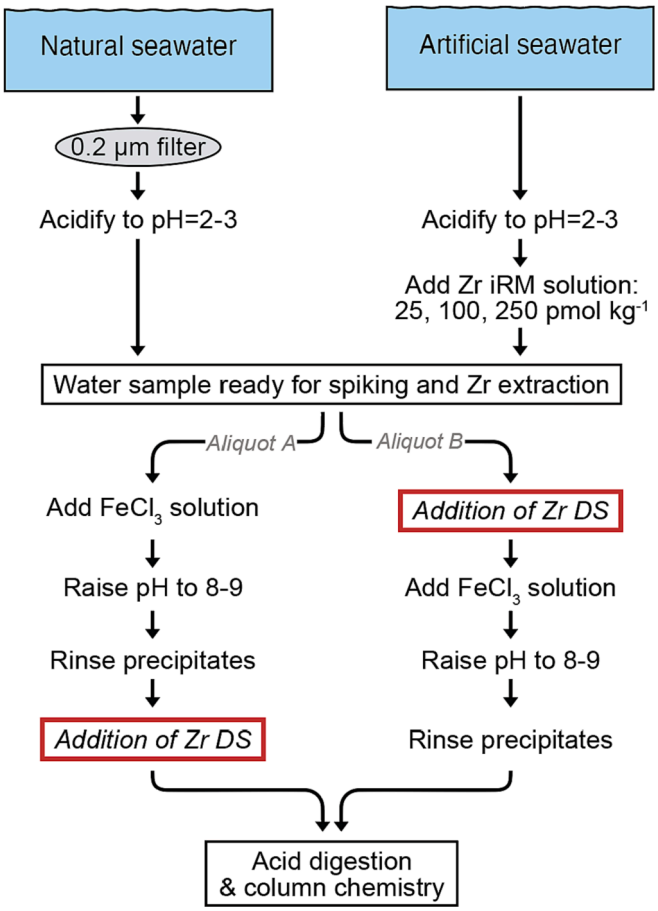

Fig. 2. Flowchart diagram indicating sample processing and analysis steps for natural and artificial seawater samples for this study.

16 M HNO_3 to remove residual HCl and evaporated to dryness before redissolution in 18 mL of 3 M HNO_3 + 0.2 M H_3BO_3 prior to chromatographic purification. All of the initial chemical processing, Fe co-precipitation, and sample digestion took place at SIO.

2.5. Test for potential systematic biases

Several parameters such as (i) the amount of Zr available for analysis, (ii) the risk of over/underspiking seawater samples with low Zr content, (iii) the timing of spiking during processing, (iv) the potential for Zr isotope fractionation during adsorption onto the Fe precipitate, and (v) potential matrix effects, can affect the accuracy of isotopic analyses. To develop a reliable Zr isotopic measurement method for water samples, we therefore investigated each of these factors. A set of experiments were designed using both synthetic (Ultrapure ≥ 99 % NaCl) and natural seawater samples.

In all experiments, a double-spike was used to correct for fractionation during sample preparation and instrumental mass-bias (Dodson, 1963; Rudge et al. 2009; Marquez & Tissot 2022). The double spike technique is well-established and widely used for the determination of high-precision Zr isotopic measurements (Ibañez-Mejia & Tissot 2019; Inglis et al. 2019; Tompkins et al. 2020). Here we used a ^{91}Zr-^{96}Zr spike, with isotopic abundances of: ^{90}Zr (5.41 %), ^{91}Zr (44.18 %), ^{92}Zr (2.90 %), ^{94}Zr (2.33 %), and ^{96}Zr (45.19 %) (Tompkins et al. 2020). Simulated mixtures of seawater with a prescribed Zr concentration (~100 pmol kg^{-1}) were prepared, and the Zr double-spike was added either before or after Fe co-precipitation (Fig. 2, Table 2). Tests were also conducted to assess the impact of over/underspiking, as well as the lower limits of sample concentration (and hence the lower limit on natural seawater volume during sample collection) for effectively isolating and measuring Zr isotopic compositions.

The first experiment aimed at assessing the impact of the timing of spiking relative to the Fe co-precipitation step, and thus whether any Zr isotope fractionation occurs during adsorption to Fe oxyhydroxides in the laboratory. For this test, several samples were split into two separate aliquots, one of which was spiked before Fe co-precipitation, and the other one spiked after. One of such pairs was a synthetic water sample doped with RM8299 Zr, and the other four pairs were natural samples (Table 2 and Fig. 2). The second series of tests aimed at assessing the impact of variable Zr concentration and processed water volumes on our method. For this test, artificial seawater samples with Zr concentration varying from 25 pmol kg^{-1} to 250 pmol kg^{-1} (fixed volume of 10 L), and with volumes varying from 6 to 14 L (fixed concentration of 100 pmol kg^{-1}), were prepared. A third experiment was designed to assess the impact of the large total dissolved solids matrix of seawater samples on our methods. For this test, solutions of both 3.5 % NaCl solution and pure MQ water (both at fixed volume of 10 L) were doped with 100 pmol kg^{-1} of RM8299 Zr, allowed to equilibrate, and then spiked with the ^{91}Zr-^{96}Zr tracer. The same Fe co-precipitation and chemical purification steps were then performed on all solutions.

To complement the extensive testing done on synthetic seawater described above and ensure the accuracy of our data on natural seawater, most natural seawater samples reported here were prepared in duplicates, with one aliquot spiked before, and the other aliquot spiked after, Fe co-precipitation. The samples were then processed fully independently through re-dissolution, column chemistry and Zr isotopic analysis.

2.6. Ion exchange chromatography

Zirconium purification was performed in the AHIL clean lab at the University of Arizona using a three-step procedure using TODGA and AG1-X8 columns, modified after Ibañez-Mejia & Tissot (2019) and Tompkins et al (2020). The first stage of column chemistry was specifically designed to isolate Zr from the major elements within the sample matrix (Fe, Al, Ca, Mg, Cr, Ti), and used 2 mL cartridges of pre-packed Eichrom DGA resin (50–100 µm particle size). The major modification in our protocol relative to previous studies is that, to avoid saturation of the resin, the 18 mL of sample solutions were loaded in 2 mL increments, in between which rinsing steps for Fe (3 M HNO_3) and Ca (12 M HNO_3) were performed (see Table 3).

The second and third columns were designed to completely isolate Zr from the residual major and trace elements within the sample matrix, including molybdenum (Mo) which has direct isobaric interferences on ^{92}Zr, ^{94}Zr, and ^{96}Zr from ^{92}Mo, ^{94}Mo, and ^{96}Mo. New, pre-cleaned Bio-Rad AG1-X8 resin (200 to 400 µm mesh) was loaded onto custom-made FEP 'micro-columns'(L = 1.6 cm; ϕ = 2 mm) with a reservoir volume of 1.6 mL.

Samples were processed following the steps shown in Table 3 using a vacuum box for the TODGA chemistry (~1 mL/min flow rate), and gravity-driven flow for the AG1-X8 steps. After chemistry, the purified Zr cuts were dried down on the hotplate at 130° C, fluxed for 3 h in 2 mL of a 15 M HNO_3 + 30 wt% H_2O_2 mixture to decompose organic residues from the resin, then dried down again, and dissolved in 1 mL of 8 M HNO_3 + 14 M HF. Once completely re-digested, samples were slowly evaporated to near dryness, and diluted into 2 mL of 0.59 M HNO_3 + 0.28 M HF, at which point they are ready for isotopic analysis.

2.7. Mass spectrometry and data treatment

Zirconium isotopic compositions were measured using a Thermo Scientific Neptune Plus MC-ICP-MS at the Isotoparium. Measurements were made in low mass resolution mode using regular sample and skimmer cones, and a static cup configuration monitoring masses 90 through 98. The cup configuration and other mass spectrometry details

Table 3
Column chemistry procedure for Zr purification from seawater samples used in this study. Table 3a. shows the procedure for the first stage column using DGA resin. Table 3b. and 3c. shows the procedure for the second and third stage columns using AG1 X8 resin (200–400 mesh).

a. First stage column (TO-DGA)

Step	Reagent	Volume (mL)	Notes
Resin cleaning	3 M HNO_3 + 0.3 M HF	15	
	3 M HNO_3 + 1 % H_2O_2	10	
	3 M HNO_3	10	
	MilliQ water	4	
Precondition 1	3 M HNO_3	10	
Sample load 1	3 M HNO_3 + 0.2 M H_3BO_3	2	* indicates repeat entire sequence 3 times
Rinse Fe	3 M HNO_3	5	*
Sample load 2	3 M HNO_3 + 0.2 M H_3BO_3	2	*
Rinse Fe	3 M HNO_3	5	*
Sample load 3	3 M HNO_3 + 0.2 M H_3BO_3	2	*
Rinse Fe	3 M HNO_3	3	*
Rinse Ca	12 M HNO_3	3	*
Re-condition	3 M HNO_3	3	*
Rinse Matrix	3 M HNO_3	20	
Elute Ti-Mo	12 M HNO_3 + 1 % H_2O_2	3.5	
Clean Fe	3 M HNO_3	20	
Elute Zr-Hf	3 M HNO_3+ 0.3 M HF	18	

b. Second stage column (AG1-X8)

Step	Reagent	Volume (mL)
Resin cleaning	6 M HCl + 0.06 M HF	1.2
	MilliQ H_2O	1.2
Precondition	7 M HF	1
Sample load	7 M HF	1
Rinse Fe-Cr	7 M HF	0.15
Rinse Fe-Cr	7 M HF	1
Elute Zr-Hf	6 M HCl + 0.06 M HF	1
	6 M HCl + 0.06 M HF	1

c. Third stage column (AG1-X8)

Step	Reagent	Volume (mL)
Resin cleaning	6 M HNO_3 + 0.2 M HF	0.8
	MilliQ H_2O	0.8
Precondition	6 M HCl + 0.06 M HF	0.8
Sample load	6 M HCl + 0.06 M HF	0.5
Elute Zr-Hf	6 M HCl + 0.06 M HF	0.1
	6 M HCl + 0.06 M HF	0.25

are included in the Table S5. Each unknown measurement was bracketed by measurements of the NIST Zr RM8299 (Tissot et al., 2023), spiked at the same level as the sample and diluted to the same concentration (within ~ 10 %). Each measurement consumed approximately 0.57 mL of solution, and each sample was measured 2–3 times, depending on the amount of Zr available for measurement.

Data processing was done offline using the minimization approach described in detail in Tompkins et al. (2020). In contrast to the conventional double-spike inversion method that uses three isotope ratios to find an exact solution to the non-linear system of equations, this method solves the double-spike equations using all five measured Zr isotopes (*i.e.*, four ratios). This over-constrained mathematical solution provides an internal check of the mass-dependency of the four isotope ratios (see Table S1).

3. Results

3.1. Notations

Zirconium isotopic variations are reported in $\delta^{94/90}Zr_{RM\ 8299}$ notation (hereafter abbreviated to $\delta^{94/90}Zr$), which is the per mil deviation of the sample $^{94}Zr/^{90}Zr$ ratio relative to NIST RM 8299 Zr iRM described in Tissot et al. (2023), as follows

$$\delta^{94/90}Zr = \left(\frac{^{94}Zr/^{90}Zr_{Sample}}{^{94}Zr/^{90}Zr_{RM8299}} - 1\right) \times 1000$$

Uncertainties for individual sample measurements are reported as 2SE (95 % CI) and calculated using the daily external reproducibility of the NIST standard (2SD) divided by the square root of the number of replicate measurements for a given sample (*i.e.*, $2SE = 2SD_{External}/\sqrt{n}$).

3.2. Yields and blanks

The procedural blank for the entire Zr chemical purification was calculated by isotope dilution using artificial seawater samples free of added Zr. Total procedural blanks and NaCl blank were found to be less than 0.3 ng of Zr, which are more than two orders of magnitude smaller than the typical Zr loads of our double spiked samples (~60–300 ng) and therefore considered negligible.

Chemistry yields were determined prior to isotopic measurements, using isotope dilution with a small (~3%) aliquot of the purified Zr fraction on the MC-ICP-MS. The calculated yields were deduced from element concentration measurements on ICP-MS at the University of California Irvine. Procedural yields of Zr using our Fe co-precipitation procedure were ~ 83 % on average, and the Zr recovery yield of the three-column separation procedure of the seawater is 86 % on average. The observed yield during the co-precipitation procedure is unlikely to be due to non-quantitative scavenging of Zr from the solution and instead may be readily attributed to minor loss of Fe-precipitates during the decanting step (up to ~ 10 %). This conclusion is supported by the fact that all synthetic seawater samples doped with the NIST Zr RM 8299 yielded $\delta^{94/90}Zr$ values undistinguishable from zero within uncertainty for all our runs. Our data shows that the incomplete collection of Zr during the co-precipitation and chemistry does not affect the measured Zr isotopic composition outside of the reported uncertainties.

3.3. Zr concentration and isotopic compositions of seawater

Without isotope dilution, it is challenging to precisely determine picomolar concentrations of dissolved Zr in seawater. An added advantage of the double-spike method is that it also allows accurate concentration determination (at the ± 1–2 % level). Indeed, using the isotopic ratios in the sample-spike mixture, the fraction of Zr (by mass) from double spike in each aliquot (Zr_{Spk}/Zr_{Tot}) can be calculated by isotope dilution (Table 4). Since the amount of Zr spike added is known, the Zr amount in the original water can be deduced, regardless of the yields from Fe co-precipitation and column chemistry. Consistent with previous studies (Godfrey et al. 1996; Firdaus et al. 2008), the Zr concentration in the natural seawater samples ranged from 24.4 to 97.5 pmol kg^{-1} (2.3–9.1 ng kg^{-1}) (Table 4). The concentration of Zr was found to be lowest at the surface (~25 pmol kg^{-1} for the 0–50 m sample) and increases with depth (50.7 pmol kg^{-1} for 300 m and 97.4 pmol kg^{-1} for 711 m).

The Zr isotopic composition for the 19 samples of artificial and natural seawater is provided in Table 4. All the artificial seawater samples have isotopic compositions indistinguishable from the NIST reference material and display a very narrow range in $\delta^{94/90}Zr$ between −0.019 ± 0.020 ‰ to + 0.014 ± 0.025 ‰. These data are discussed in Section 4.1.3 and demonstrate the accuracy and reliability of our analytical methods.

Table 4
Zirconium isotopic data of artificial and natural seawater.

Sample ID	n	Zr_{Spk}/Zr_{Tot} (%)*	[Zr] (pmol kg^{-1}) **	Zr stable isotope compositions§		Mo interference	
				$\delta^{94/90}$Zr (‰)	(±2σ)	$^{95}Mo/^{90}Zr$†	Mo/Zr (%)††
Sproul-5 m-B	2	45	24.4	1.205	0.045	1.97E-03	0.250
Sproul-5 m-A	2	53	24.4	1.196	0.045	5.36E-04	0.060
Sproul-20 m-B	2	45	25.1	1.238	0.045	7.37E-04	0.094
Sproul-20 m-A	2	54	25.1	1.287	0.045	5.90E-04	0.064
Sproul-50 m-A	2	47	26.2	1.161	0.025	5.44E-04	0.067
Sproul-300 m-B	2	46	50.8	1.481	0.025	9.68E-04	0.120
Sproul-300 m-A	2	44	50.8	1.437	0.025	6.20E-04	0.080
Sproul-711 m-B	2	50	97.5	1.528	0.030	3.22E-04	0.038
Sproul-711 m-A	2	45	97.5	1.433	0.020	3.45E-04	0.043
Seawater 1-B	2	44	~100.0	−0.011	0.020	1.38E-04	0.018
Seawater 2-A	2	42	~100.0	−0.008	0.020	1.48E-04	0.018
Surface water	2	42	~25.0	0.000	0.045	7.56E-04	0.100
Bottom water	2	44	~250.0	−0.007	0.020	8.32E-05	0.011
Seawater V1	2	44	~100.0	−0.003	0.025	4.83E-04	0.062
Seawater V2	3	44	~100.0	0.005	0.025	3.17E-04	0.040
Seawater V3	2	44	~100.0	−0.019	0.020	1.45E-04	0.019
Pier seawater-B	3	28	51.9	0.647	0.025	2.01E-04	0.032
Pier seawater-A	3	48	51.9	0.658	0.025	2.14E-04	0.026
Freshwater	3	41	~100.0	0.014	0.025	2.48E-04	0.033

* Fraction of Zr (by mass) from double spike in the spike-sample mixture, calculated by isotope dilution
** The standard deviation of [Zr] results are within 3%.
§ Uncertainties reported for each sample are 2SE, calculated using the daily external reproducibility of the NIST Zr RM8299 standard (2SD) divided by the square root of the number of replicates measured for each sample (*i.e.*, $2SE = 2SD_{External}/\sqrt{n}$).
† Ratio of measured ion beam intensities.
†† Percent Mo/Zr (atomic).

In addition to their systematic Zr concentration variations, the natural seawater samples analyzed in this study display large variation in $\delta^{94/90}$Zr values, ranging from $\delta^{94/90}$Zr of + 0.647 ± 0.025 ‰ to + 1.528 ± 0.030 ‰. The Pier seawater sample, collected at the SIO coastal research pier in San Diego, California, USA (32° 51′ 56″N 117° 15′ 13 W), has an average $\delta^{94/90}$Zr value of + 0.653 ± 0.018 ‰ (2 SE; n = 6), which is notably heavier than that of average continental clastic sediments (at ~ 0.009 ‰) (Klaver et al. 2021). Both significant and resolvable variation of Zr isotopic composition exists within the seawater profile (see Section 4.2). Further offshore, the 0–5 m surface seawater sample has an average $\delta^{94/90}$Zr value of + 1.201 ± 0.032 ‰ (2 SE; n = 4). At 20 m depth, the seawater is characterized by a $\delta^{94/90}$Zr value of + 1.263 ± 0.032 ‰ (2 SE; n = 4), and at 50 m depth, +1.161 ± 0.045 ‰ (2 SE; n = 2). A deeper seawater sample collected at 300 m has a higher $\delta^{94/90}$Zr value of + 1.459 ± 0.018 ‰ (2 SE; n = 4) and the deepest sample in our set, collected at 711 m, has a $\delta^{94/90}$Zr values of + 1.528 ± 0.030 ‰ (2 SE; n = 2).

4. Discussion

4.1. Accuracy of Zr stable isotope results

4.1.1. Achievable precision for sample-limited measurements

Because the dissolved Zr concentration in the surface ocean is typically less than 50 pmol kg^{-1} (4.6 ng kg^{-1}) (Firdaus et al. 2008; Firdaus et al. 2011), the amount of Zr that can be concentrated from seawater will inevitably be lower than the normal ~ 300 ng of Zr used for high-precision MC-ICP-MS analysis (Tompkins et al. 2020). To evaluate the precision and accuracy of $\delta^{94/90}$Zr values obtained under low Zr beam intensity conditions, we measured reference materials at three different Zr concentrations: 7, 23, and 57 ng g^{-1}, yielding mean ^{90}Zr beam intensities of ~ 0.9 V, 2.5 V and 7 V, respectively. For these tests, the spike-to-sample ratios were optimal (*i.e.*, ~0.45:0.55).

As shown in Fig. 3a, the $\delta^{94/90}$Zr values of the SPEX, IPGP and AMES pure Zr solutions for the three ^{90}Zr beam intensities (7 V, 2.5 V and ~ 0.9 V from left to right) are in excellent agreement with their published reference values (Tissot et al. 2023). As expected, the uncertainty of repeat measurements is lowest at higher Zr concentration. Importantly, the achieved uncertainties are close to the theoretical limit of precision predicted from counting statistics and Johnson noise (Fig. 3b and table S2). Going from 7 V to 2.5 V of ^{90}Zr increases the uncertainty from ± 0.021 ‰ (2SD) to ± 0.040 ‰ (2SD) respectively, and at the lowest ^{90}Zr beam intensity of 0.9 V tested, the uncertainty reaches ± 0.087 ‰ (2SD). Even at the lowest ^{90}Zr beam intensity, the Zr isotopic values obtained did not show any systematic $\delta^{94/90}$Zr bias, indicating that low level Zr isotopic analysis is robust using our methods. These results demonstrate that despite the decrease in precision, measurements remain accurate even at the low beam sizes imposed by the low Zr concentration of seawater. Given the range and variability of δ^{94}Zr values observed in seawater (see Section 4.1.3), our tests indicate that it is ideal to perform Zr isotopic measurements at ^{90}Zr beam intensity of 0.9 V or higher to ensure that precision and accuracy are better than ± 0.100 ‰.

4.1.2. Sensitivity to under/over-spiking

The double-spike method is commonly used for elements with four isotopes or more, including Zr, to perform high accuracy measurements of mass-dependent isotopic variations (Dodson, 1963; Rudge et al. 2009; Marquez & Tissot 2022). To maximize precision and minimize error, this technique requires appropriate sample to spike proportions (Millet & Dauphas, 2014; Feng et al., 2020; Tompkins et al., 2020). Given the low dissolved Zr concentration in seawater (McKelvey & Orians 1993; Firdaus et al. 2008), avoiding under/over spiking is challenging, and it is important to assess the sensitivity of the inverted $\delta^{94/90}$Zr values when optimal spiking ratio is not achieved.

Tompkins et al. (2020) showed through numerical calculations that the best spiking level for the ^{91}Zr-^{96}Zr double spike used in this study was Zr_{Spike}/Zr_{Total} ~ 45 %, and that reliable data should be obtained over a wide range of Zr_{Spike}/Zr_{Total}, from 25 % to 65 % (Tompkins et al. 2020). Because of the (*a priori*) unknown Zr concentrations in natural seawater samples, we used the depth vs. concentration relationship of The Periodic Table of the Elements in the Ocean (PTEO) to estimate the spike mass needed for our seawater samples (Bruland, 1983; Byrne, et al. 1988). The spiking levels we achieved using this approach varied from 28 % to 54 %, which are all within the robust spiking range determined by Tompkins et al. (2020). To further demonstrate that such spike-to-

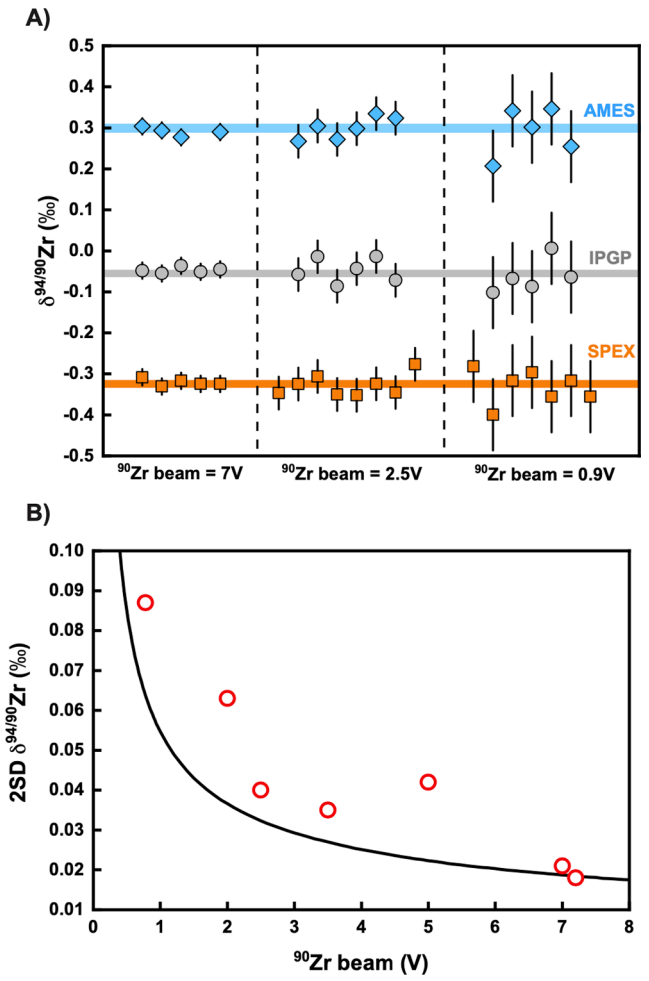

Fig. 3. A) Measurements of pure Zr reference materials at different ^{90}Zr beam intensities. The ^{90}Zr beam intensities corresponding to the data points are 7 V, 2.5 V and 0.9 V from left to right. The shaded regions represent the reported reference values for each standard from Tissot et al., (2023). B) Comparison of the measured (red circles) and predicted (solid curve) 2 SD uncertainties of $\delta^{94/90}$Zr as a function of ^{90}Zr beam intensity. The predicted curve was obtained by counting statistics and Johnson noise calculations (Dauphas et al. 2014). To account for bracketing effects, the uncertainty from the sample and bracketing standard measurement must be added in quadrature, approximated by multiplying the values by the square root of 2. The measured values are represented by the red circles are from the analyzed samples. (For interpretation of the references to color in this figure legend, the reader is referred to the web version of this article.)

sample ratios did not bias the $\delta^{94/90}$Zr values we obtained, additional analysis were performed on reference materials with variable spike-to-sample ratios within a similar but slightly larger range, from 23 % to 65 %. The under/overspiked solutions were measured as unknowns and bracketed with a standard solution spiked at the optimal level. As shown in Fig. 4, identical Zr isotope compositions were obtained over the entire range of spike-to-sample ratio tested within analytical uncertainty. This confirms that the spiking range predicted as robust by Tompkins et al. (2020) using our spike is valid, and that the spiking levels of natural samples in this study produce reliable $\delta^{94/90}$Zr data.

4.1.3. Timing of spiking, fractionation during co-precipitation, and matrix effects

Beyond the purely instrumental factors tested above, the Fe co-precipitation method used in this study to scavenge Zr and other HFSEs out of solution, has the potential to introduce systematic bias in the data through procedural isotope fractionation. However, we are not aware of any study having quantified, or even tested, the extent of HFSE isotopic fractionation during Fe co-precipitation. This is of particular interest here, since adsorption of dissolved Zr onto sinking particulates through the water column is one of the hypothesized mechanisms by which shallow waters could become depleted in Zr (Firdaus et al. 2011; Frank, 2011). To determine how this pre-concentration step may influence the measured Zr isotopic composition, three types of experiments were conducted.

As shown in Table 4 and Fig. 5, the Zr isotopic analysis of all artificial seawater and MQ water return $\delta^{94/90}$Zr values indistinguishable from that of the Zr iRM with which they were doped (within ± 0.025 ‰). These results indicate that the co-precipitation step, the initial Zr concentration of the solution, and the sample matrix, have no resolvable impact on the measured seawater Zr isotopic composition at the reported level of precision. Since the range of parameters tested here encompasses the observed range in the natural samples analyzed, these results testify to the accuracy of our approach for seawater Zr isotope analysis within our analytical precision.

4.2. Zr concentration and isotopic composition of natural seawater samples

4.2.1. Accuracy of the natural seawater Zr isotope data

As shown in Fig. 6, the Zr isotopic compositions of natural seawater sample pairs spiked before and after Fe co-precipitation are remarkably consistent with each other, although some minor offsets exist. Most samples (10 out of 12) are indistinguishable within analytical uncertainty. Only two samples showed a resolvable offset, with a maximum offset magnitude of 0.094 ± 0.036 ‰ for the 711 m-depth sample pair. Although resolvable within analytical uncertainties, this offset is more than fifteen times smaller than the $\delta^{94/90}$Zr value of the sample itself, which would not compromise data interpretation. As such, although it is possible that the Fe co-precipitation might be inducing a limited magnitude of isotope fractionation through non-quantitative recovery, this magnitude is small to unresolvable within our method uncertainty. Thus, this final test strongly supports the accuracy and robustness of our method and reported natural seawater data. Nevertheless, given the potential presence of a small isotopic effect induced by the Fe co-precipitation step, we prefer the values obtained from aliquots for which spiking took place prior to Fe co-precipitation, and use these for all subsequent discussions and interpretations.

4.2.2. Zr concentration and isotopic depth profiles

As shown in Fig. 7, Zr concentrations in the natural seawater samples studied here are lowest at the surface (~25 pmol kg^{-1} for the 0–50 m sample) and increase with depth (50.8 pmol kg^{-1} for 300 m and 97.5 pmol kg^{-1} for 711 m). This profile is consistent with previous studies (McKelvey & Orians 1993) which have suggested that Zr is particle reactive and that its concentration is generally affected by scavenging and removal in the surface ocean leading to depletion relative to deep waters (Godfrey et al. 1996; Firdaus et al. 2008). The Zr isotopic profile shows a strikingly similar structure to the Zr concentrations, with $\delta^{94/90}$Zr values increasing from ~ +1.2 ‰ near the surface to ~ +1.5 ‰ at 711 m depth. These data show, for the first time, that Zr in the dissolved fraction of seawater is strongly isotopically fractionated, with $\delta^{94/90}$Zr values much higher than those typical of igneous rocks and minerals, and of detrital sediments (Ibañez-Mejia & Tissot 2019; Klaver et al. 2021; Tian et al. 2021).

4.2.3. Possible drivers of Zr isotope fractionation in seawater

Dissolved Zr and Hf concentrations in seawater closely track that of silicate, except that dissolved Zr has markedly high concentrations in bottom water (Firdaus et al. 2011). One hypothesized mechanism for the higher observed Zr concentrations at depth in the Pacific Ocean is the dissolution of dust particles in the surface water and rapid transport to bottom water, via particulate settling and/or advection, resulting in the

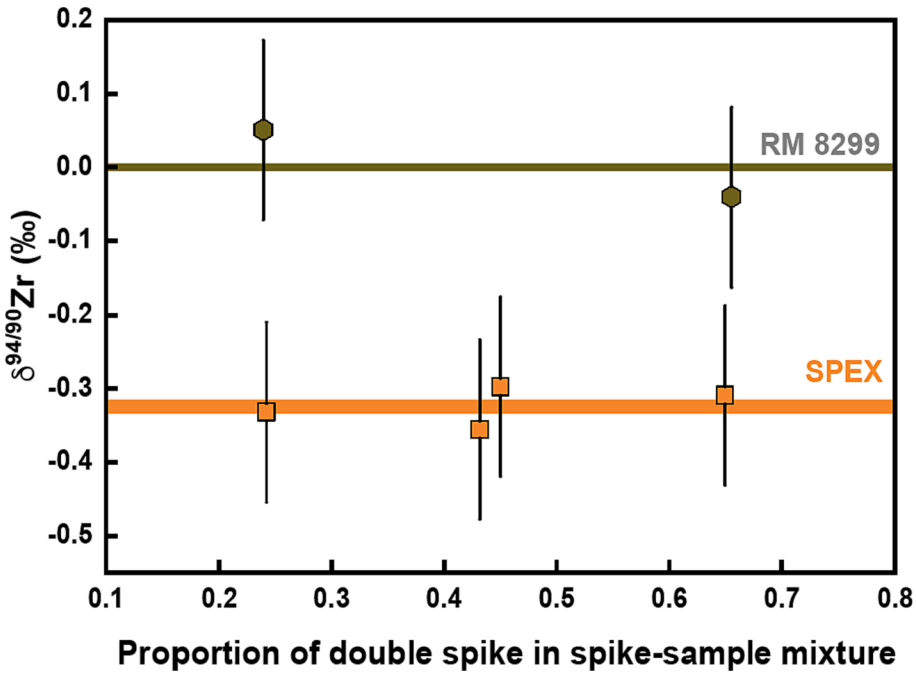

Fig. 4. Measurements of reference materials with variable spike to sample ratios, performed with a ^{90}Zr beam intensity of 0.9 ± 0.1 V. The horizontal bars represent the reported reference values and their uncertainties (Tissot et al., 2023).

high concentration in bottom water in the North Pacific (Firdaus et al. 2011). The dissolved Zr/Hf concentration ratio for seawater, which varies between 45 and 350, can deviate significantly from the chondritic Zr/Hf weight ratios of ~ 35 to 40 in detrital sediments (David et al. 2000; Tian et al. 2021). These findings suggest that water masses are preferentially retaining dissolved Zr over Hf, which may be a byproduct of different removal rates/mechanisms. The geochemical variability of dissolved Zr in seawater may be reflective of its source and residence time in the ocean, potentially making this element and its stable isotopes a useful tracer of water masses.

Since the main source of Zr to the ocean, the continental crust, has a mostly uniform Zr isotopic composition with a $\delta^{94/90}$Zr close to zero (Klaver et al. 2021; Tian et al. 2021), the highly positive $\delta^{94/90}$Zr values and fractionated depth profile of seawater must be the result of processes taking place in the hydrosphere. This includes potential fractionation during riverine transport, within the ocean itself, or a combination thereof. Our data show that the seawater $\delta^{94/90}$Zr values are well correlated with Zr concentration, and even more strongly with salinity. The surface water (0–50 m) is characterized by low concentration of Zr (~25 pmol kg^{-1}), low salinity (~33.61) and the lowest $\delta^{94/90}$Zr in our depth profile (~ +1.20 ‰) compared to other samples (Fig. 7 and table S3). The salinity and Zr concentration increase rapidly with depth to reach a maximum of 34.35 and 97 pmol kg^{-1} respectively in the bottom water (~700 m), coinciding with the largest observed $\delta^{94/90}$Zr value (+1.53 ‰) (Fig. 7b). The exact mechanisms of Zr isotope fractionation in the ocean, *i.e.*, those responsible for the on-average positive seawater $\delta^{94/90}$Zr compared to detrital sources (e.g., sediments/shales) as well as the underlying cause of the down-depth $\delta^{94/90}$Zr variation in the vertical seawater profile, are still unclear. Because the Zr isotopic composition of seawater covaries with both large-scale oceanic properties such as salinity, O_2, and temperature (Figure S2) as well as local scale properties such as beam attenuation and chlorophyll-a fluorescence (Figure S2) it is currently difficult to disentangle the exact mechanism controlling the $\delta^{94/90}$Zr variations measured in this study. Two hypotheses for this fractionation, which will be explored in more detail below, include either particle scavenging (e.g., biological productivity), or the age of water masses. Our inability to distinguish between the two processes may be a result of the limited sample size we have here and our lack of particulate data.

One possible mechanism to explain the systematically positive $\delta^{94/90}$Zr in seawater is scavenging from the dissolved Zr load onto sinking particulates throughout the water column. In this framework, Zr is rapidly removed from solution by surface interactions with sinking particles (Firdaus et al. 2011; Censi et al. 2018), resulting in the lower dissolved Zr concentration in the surface water (Fig. 7a). Preferential removal of light Zr isotopes during scavenging could then result in the on-average positive $\delta^{94/90}$Zr we measured in seawater. If Zr scavenging takes place following a closed-system Rayleigh-type mechanism down-depth, significant Zr isotopic variations could be observed in different fractions (dissolved and particulate) as Zr removal occurs from seawater. This mechanism is at odds, however, with the observation that deeper samples in our vertical profile have higher Zr concentrations, and with the interpretation that the down-depth increase in [Zr] and $\delta^{94/90}$Zr shown in Fig. 7a represents a vertical scavenging profile. This is because, if a down-depth Rayleigh-type fractionation was at play, preferential removal of light Zr isotopes in the shallow ocean would result in an inverse correlation between [Zr] and $\delta^{94/90}$Zr of the dissolved load down depth, which is the opposite of what is observed in our profile. Moreover, the residence time of Zr in the ocean is ~ 3700 years (Firdaus et al. 2011), meaning that only a very small proportion of Zr is removed from the ocean each year. Therefore, although bulk removal of light Zr isotopes within Earth's hydrosphere seems necessary to account for the average positive $\delta^{94/90}$Zr observed in seawater relative to the upper continental crust, a simple vertical Rayleigh fractionation mechanism in the ocean driven by preferential removal of light Zr isotopes via particle scavenging seems unlikely.

4.2.4. *Potential future applications of Zr isotopes in the ocean*

One possibility for explaining the observed $\delta^{94/90}$Zr variations as a function of depth in our sampling site is that both elemental Zr and its isotopes vary as a function of the water mass it originated from. Our sampling profile is located close to the Pacific Ocean continental shelf slope, where the surface California Current and subsurface California Undercurrent reflect the dominant advective pathways for two water masses: Pacific Subarctic Upper Water and Pacific Equatorial Water, respectively (Thomson & Krassovski 2010; Bograd et al. 2019). As

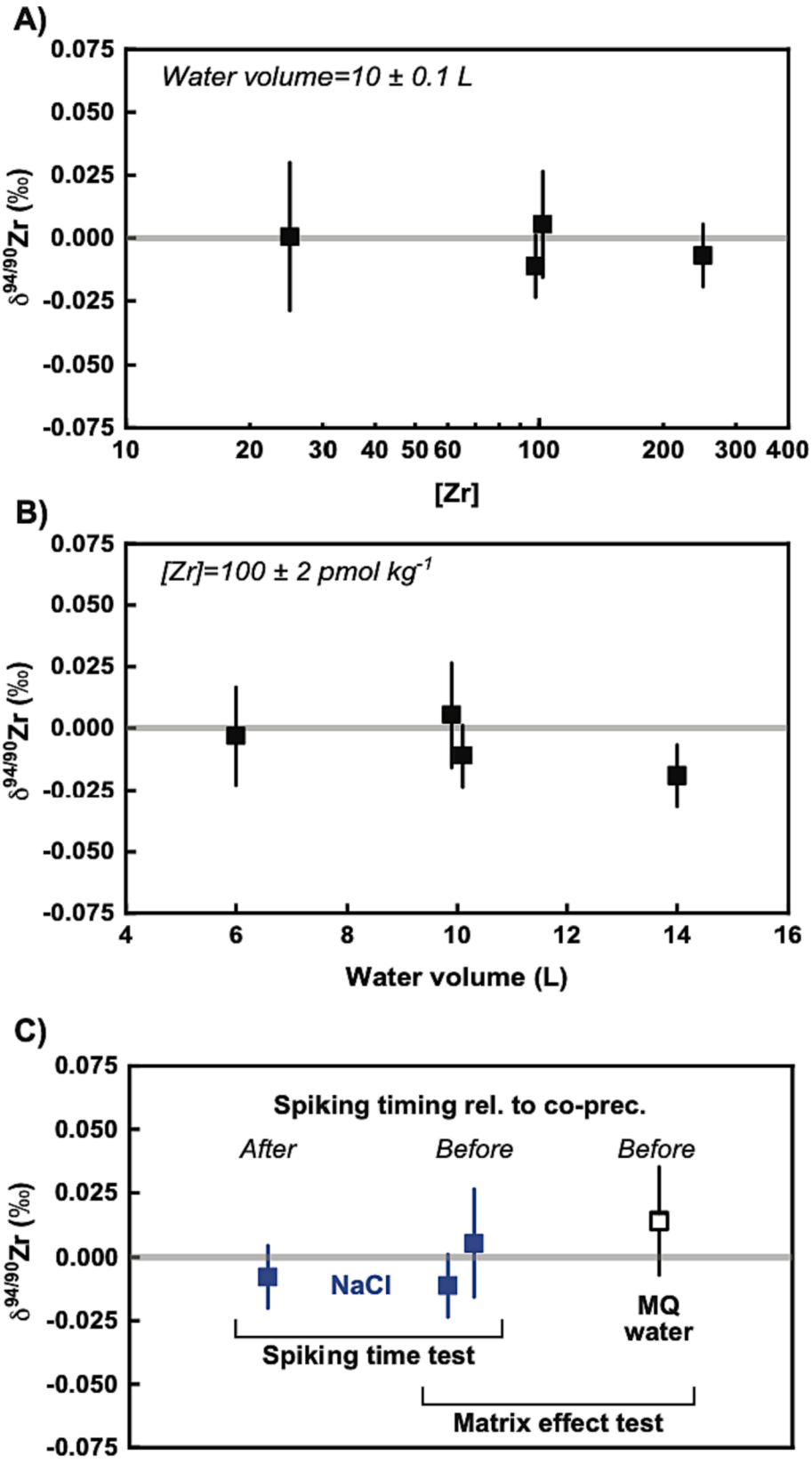

Fig. 5. Plots of $\delta^{94/90}$Zr determined in artificial seawater samples doped with RM 8299 Zr and processed under different conditions, namely A) variable Zr concentration, B) different water volumes, C) spiking before and after Fe co-precipitation, and matrix composition.

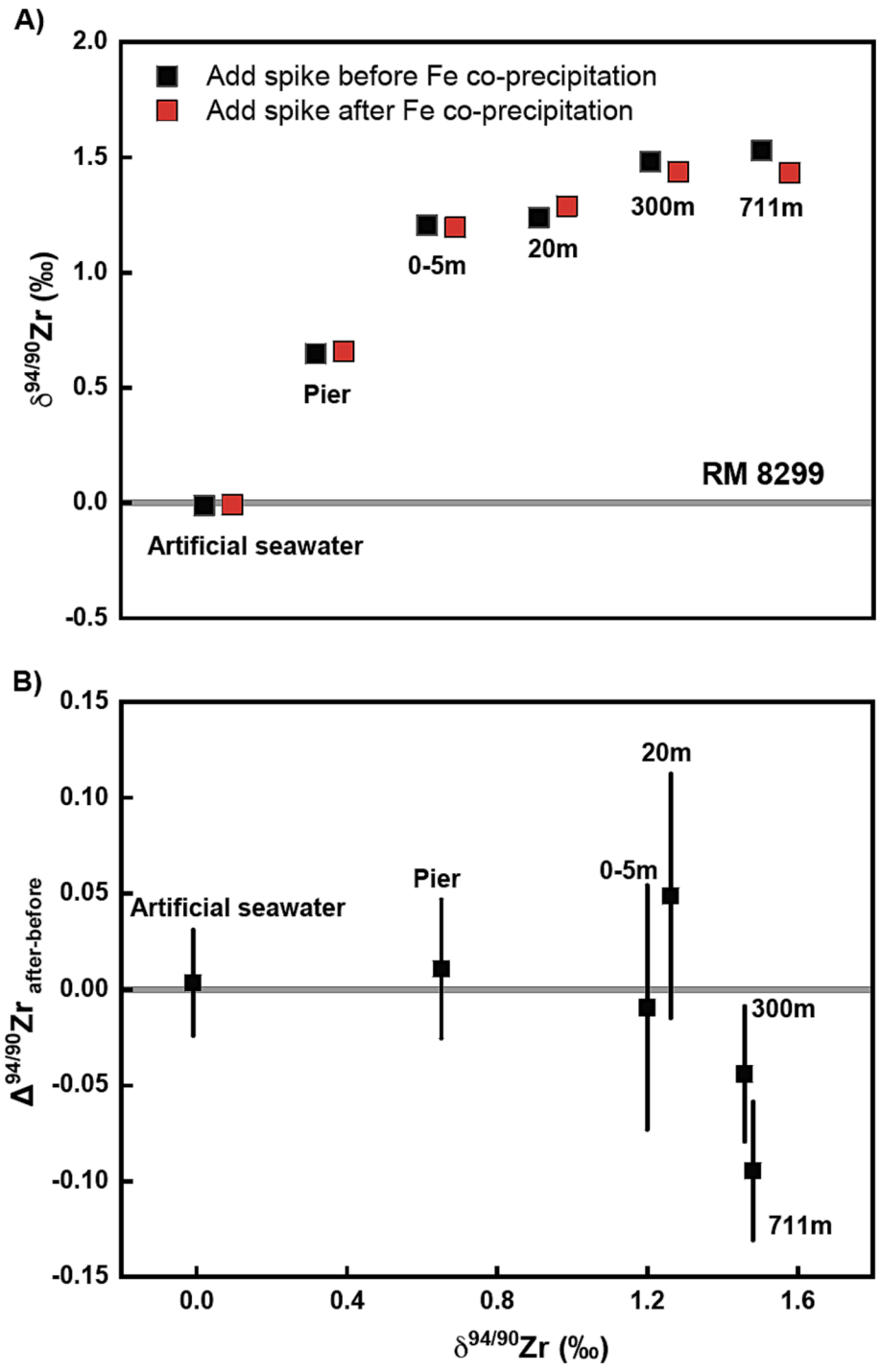

Fig. 6. Plots of Zr isotopic measurements of seawater samples processed under different spiking conditions. A) Zr isotopic compositions in seawater. Black squares are sample aliquots spiked before Fe co-precipitation and red squares are aliquots spiked after Fe co-precipitation. Uncertainties are smaller than the symbols. B) The $\delta^{94/90}$Zr difference between aliquots of the same sample spiked before and after coprecipitation. The x-axis in panel B is the δ^{94}Zr of the samples spiked after iron co-precipitation $\Delta^{94/90}Zr_{\text{after-before}} = \delta^{94/90}Zr_{\text{after}} - \delta^{94/90}Zr_{\text{before}}$. (For interpretation of the references to color in this figure legend, the reader is referred to the web version of this article.)

shown in Fig. 8a, these two water masses are well identified by the potential temperature-salinity relationship. The California Current is characterized by a low-density layer located above isopycnal surface $\sigma_\theta = 25.8$ kg/m^3 (*i.e.*, the pycnocline), whereas the California Undercurrent below is relatively cold with a high density ($\sigma_\theta > 26$ kg/m^3) (Bograd et al. 2019). In the profile studied here, the surface water where the California Current is a major contributor to water masses above the pycnocline is characterized by relatively lighter $\delta^{94/90}$Zr values compared to deeper water. The highest $\delta^{94/90}$Zr values correlate to the highest salinity, which are found closer to the profile bottom, where the deeper water mass is dominant in this layer.

In situ observations of beam transmission are often used as a proxy for particle mass or volume in the water column (Pak & Zaneveld, 1977), which in turn can be used as an indicator of suspended particulate matter. We show that the observed Zr isotopic composition of the dissolved fraction of seawater is well correlated with that of beam

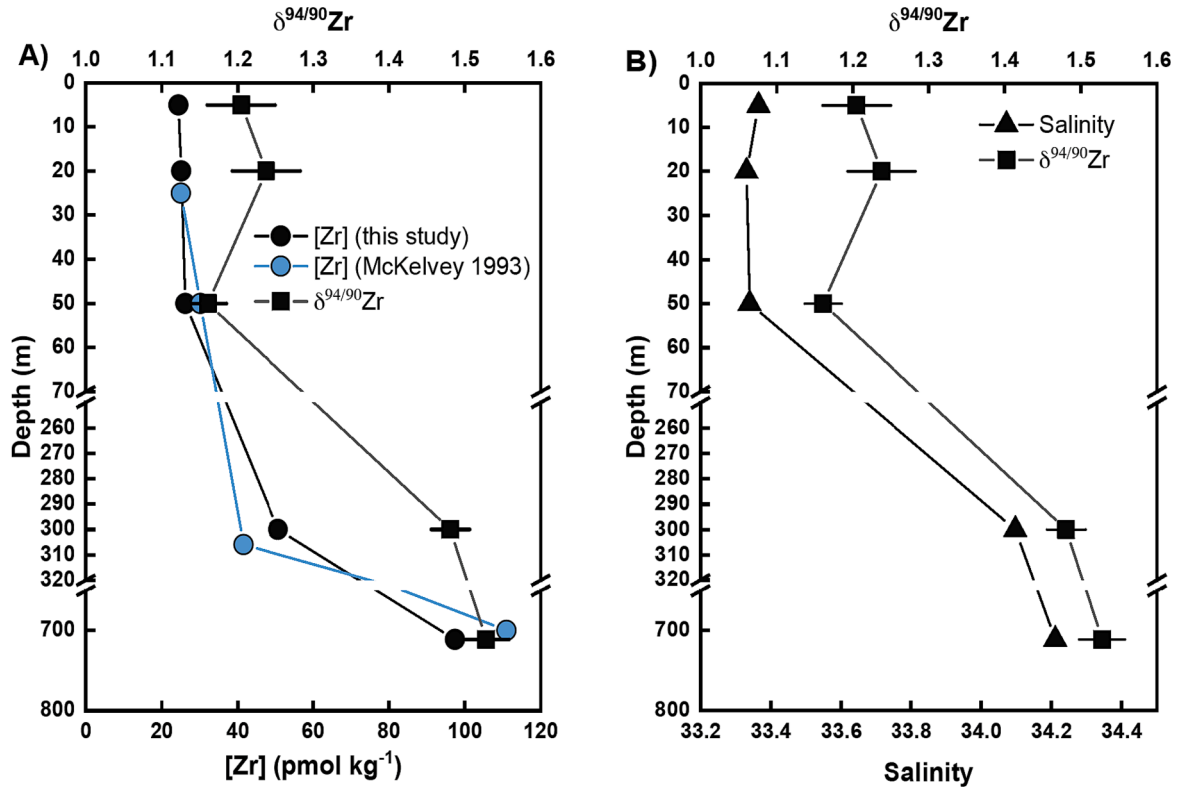

Fig. 7. A) Zirconium concentration, and B) Salinity and Zr isotopic composition in a vertical seawater profile in the East Pacific Ocean. On both panels, $\delta^{94/90}$Zr values are from samples spiked before Fe-coprecipitation. The blue circles in panel A represent the Zr concentration data from McKelvey & Orians 1993. (For interpretation of the references to color in this figure legend, the reader is referred to the web version of this article.)

transmission (Fig. 8b), with generally lighter Zr isotopic compositions of seawater observed at depths with high particle mass/volume. The fluorescence data during sample collection indicates a maximum close to 40 m depth (Fig. 8b), which corresponds to the lowest $\delta^{94/90}$Zr value observed in our seawater profile. The subsurface chlorophyll maximum is coincident with the minimum in beam transmission (Fig. 8b) which indicates the high volume of particulates in the upper water column are biogenic in origin. If adsorption of Zr onto particulates in the water column were the underlying mechanism responsible for the trends in seawater we observe here, this would require the heavy Zr isotopes to preferentially adsorb onto particles leaving behind lighter seawater as observed towards the top of the water profile. As these particulates settle through the water column, reverse weathering of Zr from the particulate fraction could possibly release this isotopically heavy Zr to produce a pattern that is consistent with what we observe near the bottom of the water column (Fig. 8b). This hypothesis could be verified by measuring the Zr isotopic composition of sinking particulate matter from different depth horizons. While the origin of the variable Zr isotope composition throughout the water column remains to be mechanistically explained, our results suggest that the combination of salinity, Zr concentration, and Zr isotopes may serve as a new and promising tool to trace water masses in the ocean. If the process controlling Zr isotopic fractionation in the water column is due to particle scavenging of dissolved Zr and it follows a Rayleigh or steady state fractionation process, it is possible that Zr isotopic compositions could be used as a proxy for biological productivity.

The results presented here provide the very first insights into the behavior of Zr stable isotopes in Earth's hydrosphere and the ocean system, thus allowing us to begin developing an oceanographic understanding of the importance of $\delta^{94/90}$Zr variations in marine systems. Although additional work is needed to better understand the mechanisms driving Zr isotope fractionation in the oceans before these variations can be interpreted robustly, the method we present here provides a robust tool to investigate them within the ocean. Based on the limited number of natural seawater samples analyzed here, we have no clear evidence to show that the fractionated $\delta^{94/90}$Zr values can be explained by open-system fractionation at steady state, closed-system Rayleigh fractionation, or two-component mixing (Fig. S3). Future detailed investigations should ideally include: i) measurement of $\delta^{94/90}$Zr values in multiple vertical profiles spanning diverse settings and water masses to test the water mass mixing hypotheses; ii) investigating processes at the land–ocean boundary, such as river runoff, submarine groundwater discharge, hydrothermal fluids, and constraining the range of $\delta^{94/90}$Zr values for these potential sources and sinks; iii) collecting marine particles and dissolved seawater in tandem to constrain the metal scavenging fractionation factor.

5. Conclusions

In this study we have established a new method for determining the stable Zr isotope composition ($\delta^{94/90}$Zr) of water samples with high accuracy and precision, using a combination of Fe co-precipitation and the double-spike method with a modified three-column ion exchange chromatography. The influence of Fe co-precipitation, sample matrix, spike-to-sample ratio, and Zr concentration on $\delta^{94/90}$Zr analysis, were all tested to verify the accuracy and reliability of the data. We found that the yield of our entire procedure is consistently high (>70 %), and that this non-quantitative recovery does not influence the measured $\delta^{94/90}$Zr outside of analytical uncertainties. Using this new method, we measured the Zr isotopic composition of coastal seawater from La Jolla, CA, and of a vertical water profile in the nearshore Pacific Ocean around the latitude of Southern California. Natural seawater samples display large $\delta^{94/90}$Zr variations, ranging from + 0.65 to 1.53 ‰ and, in our vertical transect, varying as a function of water depth. Variations with depth are well correlated with Zr concentrations and total salinity, indicating that an underlying mechanism capable of strongly fractionating Zr isotopes

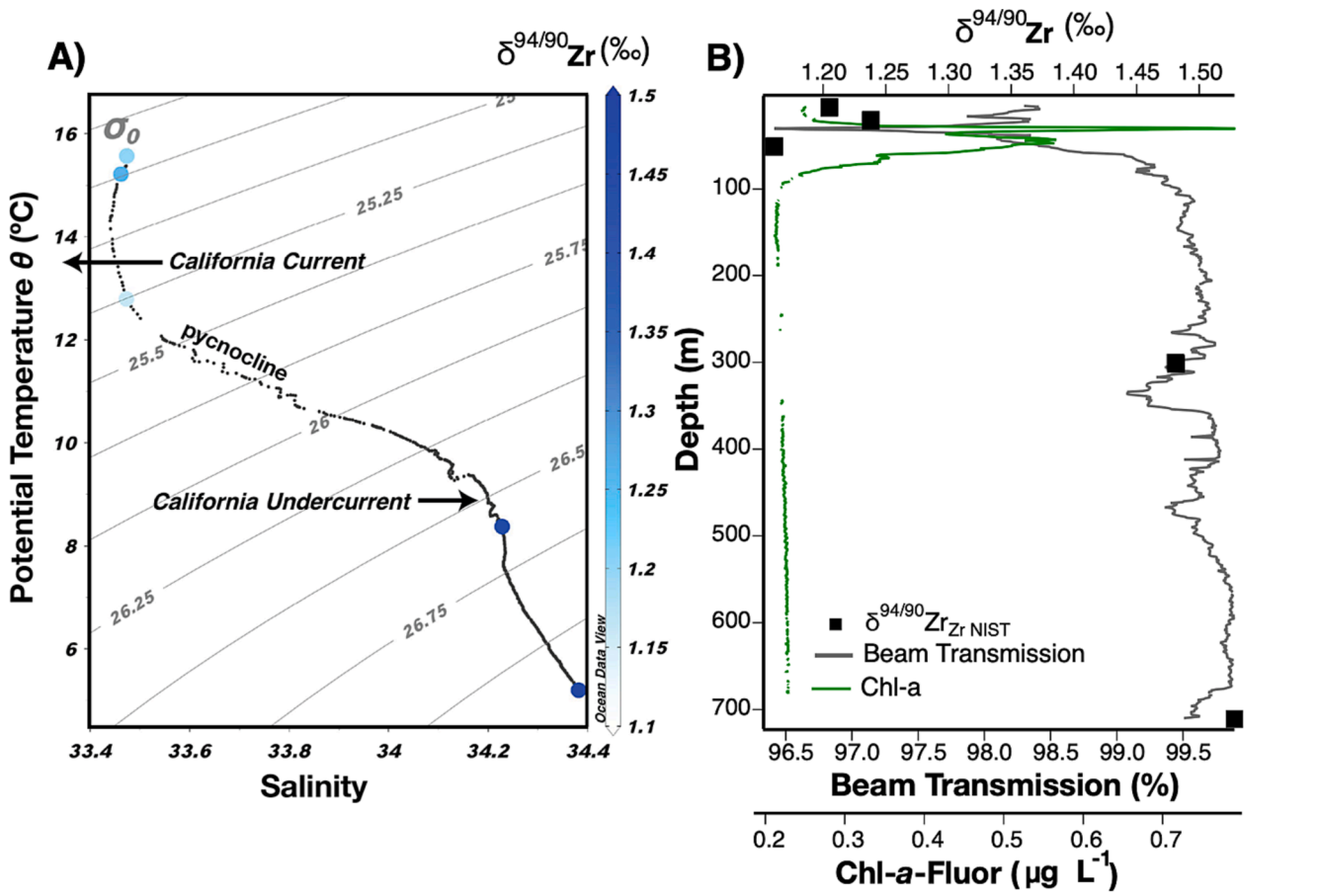

Fig. 8. A) Potential temperature (θ) vs. Salinity (S) diagram with major advective pathways for source surface and subsurface water masses offshore southern California indicated by arrows. Color bar indicates the $\delta^{94/90}$Zr values. The black dots represent the hydrographic profile for the sampled station and contours (sigma-theta) are lines of constant density with units kg m^{-3}. B) Beam transmission data (gray line) and Chlorophyll-a fluorescence data (green line) for the sampled profile and the $\delta^{94/90}$Zr values of the dissolved seawater fraction. (For interpretation of the references to color in this figure legend, the reader is referred to the web version of this article.)

in the hydrosphere exists. Our results suggest that Zr isotopes might be strongly fractionated by reactive particle scavenging in the oceans, and that seawater $\delta^{94/90}$Zr variations may serve as a new tracer of water masses. However, more work is needed on ocean profiles with contrasting water masses from multiple localities, to better understand and disentangle the underlying mechanisms behind these fractionations and to better interpret their significance.

Data availability

Data are available through Mendeley Data at https://doi.org/10.17632/84y45dsp28.3.

Declaration of competing interest

The authors declare that they have no known competing financial interests or personal relationships that could have appeared to influence the work reported in this paper.

Acknowledgments

We acknowledge support for this project from the University of California San Diego Academic Senate, startup funds provided to S.M. Aarons, and the Devendra and Aruna Lal Fellowship awarded to L. Huang. This work was further supported by NSF-EAR grants 2131632 and 2143168 (to MIM), and 1824002 (to FLHT). FLHT acknowledges additional support from NSF grant MGG-2054892, a Packard Fellowship, a research award from the Heritage Medical Research Institute, and startup funds from Caltech. The authors thank E. Norris and R. Blankenship for assistance with SIO Pier water sample collection, R. Chen for CTD data processing, and M.A. Kipp for assistance with some Zr isotopic measurements at Caltech. Careful reviews by R.C. Xie, T.J. Horner and one anonymous reviewer greatly improved the study. Executive Editor J.G. Catalano and Associate Editor Y. Sohrin are thanked for efficient handling of the manuscript. Seawater collections were supported by the University of California Ship Funds Program at Scripps Institution of Oceanography, awarded to L.A. Levin and C.A. Choy. We thank the crew of the R/V *Sproul* for their assistance in sample collection at sea.

Appendix A. Supplementary material

Supplementary material for this article can be found online at https://doi.org/10.1016/j.gca.2023.11.018.

References

Aarons, S.M., Johnson, A.C., Rader, S.T., 2021. Forming earth's continental crust: A nontraditional stable isotope perspective. Elements. 17, 413–448.
Arendt, C.A., Aciego, S.M., Sims, K.W., Robbins, M., 2015. Sequential separation of uranium, hafnium and neodymium from natural waters concentrated by iron coprecipitation. Geostand. Geoanal. Res. 39, 293–303.
Bindeman, I., Melnik, O., 2022. The rises and falls of zirconium isotopes during zircon crystallisation. Geochem. Perspect. Lett. 24, 17–21.
Bograd, S.J., Schroeder, I.D., Jacox, M.G., 2019. A water mass history of the Southern California current system. Geophys. Res. Lett. 46, 6690–6698.

Bruland, K., 1983. Chemical oceanography. Academic Press, London.
Byrne, R.H., Kump, L., Cantrell, K., 1988. The influence of temperature and pH on trace metal speciation in seawater. Mar. Chem. 25, 163–181.
Censi, P., Sposito, F., Inguaggiato, C., Zuddas, P., Inguaggiato, S., Venturi, M., 2018. Zr, Hf and REE distribution in river water under different ionic strength conditions. Sci. Total Environ. 645, 837–853.
Chen, X., Wang, W., Zhang, Z., Nie, N.X., Dauphas, N., 2020. Evidence from *Ab Initio* and transport modeling for diffusion-driven zirconium isotopic fractionation in igneous rocks. ACS Earth Space Chem. 4, 1572–1595.
Claiborne, L.L., Miller, C., Walker, B., Wooden, J., Mazdab, F., Bea, F., 2006. Tracking magmatic processes through Zr/Hf ratios in rocks and Hf and Ti zoning in zircons: an example from the Spirit Mountain batholith, Nevada. Mineral. Mag. 70, 517–543.
Dauphas, N., Chen, J.H., Zhang, J., Papanastassiou, D.A., Davis, A.M., Travaglio, C., 2014. Calcium-48 isotopic anomalies in bulk chondrites and achondrites: Evidence for a uniform isotopic reservoir in the inner protoplanetary disk. Earth Planet. Sci. Lett. 407, 96–108.
David, K., Schiano, P., Allegre, C., 2000. Assessment of the Zr/Hf fractionation in oceanic basalts and continental materials during petrogenetic processes. Earth Planet. Sci. Lett. 178, 285–301.
Dodson, M., 1963. A theoretical study of the use of internal standards for precise isotopic analysis by the surface ionization technique: Part I-General first-order algebraic solutions. J. Sci. Instrum. 40, 289.
Feng, L., Hu, W., Jiao, Y., Zhou, L., Zhang, W., Hu, Z., Liu, Y., 2020. High-precision stable zirconium isotope ratio measurements by double spike thermal ionization mass spectrometry. J. Anal. at. Spectrom. 35, 736–745.
Firdaus, M.L., Norisuye, K., Nakagawa, Y., Nakatsuka, S., Sohrin, Y., 2008. Dissolved and labile particulate Zr, Hf, Nb, Ta, Mo and W in the western North Pacific Ocean. J. Oceanogr. 64, 247–257.
Firdaus, M.L., Minami, T., Norisuye, K., Sohrin, Y., 2011. Strong elemental fractionation of Zr–Hf and Nb–Ta across the Pacific Ocean. Nat. Geosci. 4, 227–230.
Frank, M., 2011. Chemical twins, separated. Nat. Geosci. 4, 220–221.
Godfrey, L., White, W., Salters, V., 1996. Dissolved zirconium and hafnium distributions across a shelf break in the northeastern Atlantic Ocean. Geochim. Cosmochim. Acta. 60, 3995–4006.
Goldschmidt, V.M., 1937. The principles of distribution of chemical elements in minerals and rocks. The seventh Hugo Müller Lecture, delivered before the Chemical Society on March 17th, 1937. Journal of the Chemical Society (Resumed), 655-673.
Guo, J.-L., Wang, Z., Zhang, W., Feng, L., Moynier, F., Hu, Z., Zhou, L. and Liu, Y. 2022. Zirconium and its stable isotopes in igneous systems. Earth Sci. Rev., 104289.
Guo, J.-L., Wang, Z., Zhang, W., Moynier, F., Cui, D., Hu, Z., Ducea, M.N., 2020. Significant Zr isotope variations in single zircon grains recording magma evolution history. Proc. Natl. Acad. Sci. u.s.a. 117, 21125–21131.
He, S., Li, Y., Wu, L.-G., Guo, D.-F., Li, Z.-Y., Li, X.-H., 2021. High precision zircon SIMS Zr isotope analysis. J. Anal. at. Spectrom. 36, 2063–2073.
Hoskin, P.W., Schaltegger, U., 2003. The composition of zircon and igneous and metamorphic petrogenesis. Rev. Mineral. Geochem. 53, 27–62.
Ibañez-Mejia, M., Tissot, F.L., 2019. Extreme Zr stable isotope fractionation during magmatic fractional crystallization. Sci. Adv. 5, eaax8648.
Inglis, E.C., Creech, J.B., Deng, Z., Moynier, F., 2018. High-precision zirconium stable isotope measurements of geological reference materials as measured by double-spike MC-ICPMS. Chem. Geol. 493, 544–552.
Inglis, E.C., Moynier, F., Creech, J., Deng, Z., Day, J.M., Teng, F.-Z., Bizzarro, M., Jackson, M., Savage, P., 2019. Isotopic fractionation of zirconium during magmatic differentiation and the stable isotope composition of the silicate Earth. Geochim. Cosmochim. Acta 250, 311–323.
Jiao, Y., Zhou, L., Algeo, T.J., Shen, J., Feng, L., Hu, Y., Liu, J., Chi, L., Shi, M., 2022. Zirconium isotopes track volcanic inputs during the Permian-Triassic transition in South China. Chem. Geol. 610, 121074.
Kelemen, P., Johnson, K., Kinzler, R., Irving, A., 1990. High-field-strength element depletions in arc basalts due to mantle–magma interaction. Nature 345, 521–524.
Klaver, M., MacLennan, S.A., Ibañez-Mejia, M., Tissot, F.L., Vroon, P.Z., Millet, M.-A., 2021. Reliability of detrital marine sediments as proxy for continental crust composition: The effects of hydrodynamic sorting on Ti and Zr isotope systematics. Geochim. Cosmochim. Acta 310, 221–239.
Marquez, R.T., Tissot, F.L., 2022. COSMO: Double spike optimization for sample-limited analyses of isotopically anomalous materials. Chem. Geol. 612, 121095.
McKelvey, B.A., Orians, K.J., 1993. Dissolved zirconium in the north Pacific Ocean. Geochim. Cosmochim. Acta 57, 3801–3805.
Méheut, M., Ibañez-Mejia, M., Tissot, F.L., 2021. Drivers of zirconium isotope fractionation in Zr-bearing phases and melts: the roles of vibrational, nuclear field shift and diffusive effects. Geochim. Cosmochim. Acta 292, 217–234.
Millet, M.-A., Dauphas, N., 2014. Ultra-precise titanium stable isotope measurements by double-spike high resolution MC-ICP-MS. J. Anal. at. Spectrom. 29, 1444–1458.
Münker, C., Wörner, G., Yogodzinski, G., Churikova, T., 2004. Behaviour of high field strength elements in subduction zones: constraints from Kamchatka-Aleutian arc lavas. Earth Planet. Sci. Lett. 224, 275–293.
Orians, K., Merrin, C., 2001. Refractory metals. Encyclopedia of Ocean Sciences 4, 2387–2399.
Pak, H., Zaneveld, J.R.V., 1977. Bottom nepheloid layers and bottom mixed layers observed on the continental shelf off Oregon. J. Geophys. Res. 82, 3921–3931.
Pfänder, J.A., Münker, C., Stracke, A., Mezger, K., 2007. Nb/Ta and Zr/Hf in ocean island basalts—implications for crust–mantle differentiation and the fate of Niobium. Earth Planet. Sci. Lett. 254, 158–172.
Rickli, J., Frank, M., Halliday, A.N., 2009. The hafnium–neodymium isotopic composition of Atlantic seawater. Earth Planet. Sci. Lett. 280, 118–127.
Rudge, J.F., Reynolds, B.C., Bourdon, B., 2009. The double spike toolbox. Chem. Geol. 265, 420–431.
Schmidt, K., Bau, M., Hein, J.R., Koschinsky, A., 2014. Fractionation of the geochemical twins Zr–Hf and Nb–Ta during scavenging from seawater by hydrogenetic ferromanganese crusts. Geochim. Cosmochim. Acta 140, 468–487.
Shannon, R.D., 1976. Revised effective ionic radii and systematic studies of interatomic distances in halides and chalcogenides. Acta Crystallographica Section a: Crystal Physics, Diffraction, Theoretical and General Crystallography 32, 751–767.
Thomson, R.E., Krassovski, M.V., 2010. Poleward reach of the California Undercurrent extension. J. Geophys. Res. Oceans 115.
Tian, S., Moynier, F., Inglis, E., Creech, J., Bizzarro, M., Siebert, J., Day, J., Puchtel, I., 2020. Zirconium isotopic composition of the mantle through time. Geochem. Perspect. Lett. 15, 40–43.
Tian, S., Moynier, F., Inglis, E.C., Rudnick, R.L., Huang, F., Chauvel, C., Creech, J.B., Gaschnig, R.M., Wang, Z., Guo, J.-L., 2021. Zirconium isotopic composition of the upper continental crust through time. Earth Planet. Sci. Lett. 572, 117086.
Tissot, F.L.H., Ibañez-Mejia, M., Rabb, S.A., Kraft, R.A., Vocke, R.D., Fehr, M.A., Schönbächler, M., Tang, H., and Young, E.D. 2023. A community-led calibration of the Zr isotope Reference Materials: NIST RM 8299 and SRM 3169. J. Anal. At. Spectrom., https://doi.org/10.1039/D3JA00167A.
Tompkins, H.G.D., Zieman, L.J., Ibañez-Mejia, M., Tissot, F.L.H., 2020. Zirconium stable isotope analysis of zircon by MC-ICP-MS: Methods and application to evaluating intra-crystalline zonation in a zircon megacryst. J. Anal. at. Spectrom. 35, 1167–1186.
Tompkins, H.G.D., Ibañez-Mejia, M., Tissot, F.L.H., Bloch, E., Wang, Y., Trail, D., 2023. Zircon growth experiments reveal limited equilibrium Zr isotope fractionation in magmas. Geochem. Perspect. Lett. 25, 25–29.
Weyer, S., Münker, C., Mezger, K., 2003. Nb/Ta, Zr/Hf and REE in the depleted mantle: implications for the differentiation history of the crust–mantle system. Earth Planet. Sci. Lett. 205, 309–324.
Wu, T., Zhang, W., Wilde, S.A., 2020. The origin of mafic microgranular enclaves in granitoids: Insights from in situ Sr isotope of plagioclases and Zr-Hf isotopes of zircons. Chem. Geol. 551, 119776.
Xie, Q., Kerrich, R., Fan, J., 1993. HFSE/REE fractionations recorded in three komatiite-basalt sequences, Archean Abitibi greenstone belt: Implications for multiple plume sources and depths. Geochim. Cosmochim. Acta 57, 4111–4118.
Xie, J.-C., Zhu, D.-C., Wang, Q., Zhang, L.-L., 2023. Zirconium isotopic composition of zircon reference materials by laser ablation multi-collector inductively coupled plasma mass spectrometry. Int. J. Mass Spectrom. 484, 116995.
Zhang, W., Wang, Z., Moynier, F., Inglis, E., Tian, S., Li, M., Liu, Y., Hu, Z., 2019. Determination of Zr isotopic ratios in zircons using laser-ablation multiple-collector inductively coupled-plasma mass-spectrometry. J. Anal. at. Spectrom. 34, 1800–1809.
Zhang, W., Hu, Z., Feng, L., Wang, Z., Liu, Y., Feng, Y., Liu, H., 2022. Accurate determination of Zr isotopic ratio in zircons by femtosecond laser ablation MC-ICP-MS with "wet" plasma technique. J. Earth Sci. 33, 67–75.
Zhu, Z., Zhang, W., Wang, J., Wang, Z., Guo, J.-L., Hoffmann, J.E., Feng, L., Luo, T., Hu, Z., Liu, Y., 2023. Magmatic crystallization drives zircon Zr isotopic variations in a large granite batholith. Geochim. Cosmochim. Acta 342, 15–30.